Cassini Data Specifically Relevant for Comparison with the Huygens Probe

Ralph Lorenz (Ralph.lorenz@jhuapl.edu)

19/6/2018

With contributions from Conor Nixon, Christophe Sotin, Zibi Turtle, Erich Karkoschka, Tommi Koskinen, Bob West, Aseel Atanabwi, Michael Malaska, McEwen, Perry and discussions with Darrel Strobel and Roger Yelle.

This note aims to summarize the Cassini data most relevant for comparison or context-setting of the Huygens probe. Some data are presented here as high-order products (mosaics of images, reconstructed profiles) and some guidance to locating the original data is given. The data are discussed in terms of surface, 'lower atmosphere' (i.e. Huygens parachute descent altitudes ~150km to the surface) and 'upper atmosphere' (150-1400km, where only the accelerometer data was recorded).

1. Surface Data

The Huygens Probe landed on 14 January 2005 (Saturn season Ls= 303 : late southern summer - solstice was in October 2002, and not long after perihelion in July 2003).The landing site coordinates were determined (e.g. [1])at the time to be Longitude 192.4 degrees W (167.6 degrees E) (+- 0.05 degrees 1 sigma or about 2.2 km) and Latitude -10.2 degrees S (+- 0.1 degrees 1 sigma or about 4.5 km). Note that the latitude/longitude reference frame onto which data products (notably RADAR swaths) was projected was revised once the rotation state of Titan was determined, in particular the obliquity of Titan's pole with respect to Titan's orbit normal had originally been assumed to be 0.0 but was measured to be 0.3 degrees [2, 3] and a possibly non-synchronous rotation rate was inferred. The impact on the Huygens coordinates is discussed by [3]. Further radar data have refined the rotation state, the apparent longitude changes being likely due to polar precession rather than nonsynchronous rotation [4]. Various analyses and products at different times may use different assumed pole positions and rotation rates, such that misregistration errors of up to about 0.3 degrees (10km) may occur if attention is not paid to mapping the data.

Huygens image comparison with RADAR data was reported by [5]: see also [6, 7] which discusses VIMS data at the large scale; [8] discusses VIMS data of the landing site in particular, acquired on flyby TA. Higher-quality VIMS data on the landing site were acquired on flyby T47, See section 2 of Appendix A.

ISS data on Titan's surface (acquired prior to the Huygens descent) is presented in [9]. A new processing scheme to integrate information from all the images acquired in the mission is underway and the resulting mosaic at the landing site is indicated in Appendix A, section 1.

Low-resolution (>50km) radar scatterometry and radiometry of the landing site was acquired on TA (e.g. [10])

RADAR imaging (SAR) of the landing site (~1km resolution) was obtained on T8 by extending the image swath beyond what had been originally planned (e.g. [11]). A small image around the landing site was also obtained by high-altitude SAR using only the central beam ('HiSAR') on flyby T13. The originally-planned SAR coverage of the landing site was acquired on T41.

The topographic information from these radar data (nearby the Huygens landing site) are compared with the Huygens radar altimeter in [12]. In particular, it may be noted that the T41 SAR topography suggests the altitude of the Huygens landing site was within about 100m of the 2575km radius assumed for Titan.

2. Lower Atmospheric Data

The local solar time of the Huygens descent was about 9am (the sun was about 40 degrees up in the sky; the subsolar latitude was 22.8 deg South). The Titan-Sun distance at the time was 9.06 AU. The Huygens descent measurements (e.g. optical measurements, direct temperatures/pressures, winds from Doppler tracking, chemical abundances etc.) began at about 150km altitude.

Clearly, because Cassini was tasked with receiving and relaying the Huygens radio signal, no absolutely simultaneous observations of Titan could be obtained. Cassini data on flybys before and after the Huygens delivery (Tc) may be at different latitudes, local solar times, magnetospheric conditions etc. Most importantly, perhaps, the increasing distance from the sun throughout the Cassini mission means that seasonal changes erode the value of comparison of data acquired after about 2008.

The radio occultation (RSS) profile of most relevance for Huygens is that of T12, published in [13]

Thermal infrared observations by CIRS have been used to retrieve temperatures and abundances, and winds. Initial results were reported by [14] – a fuller discussion of CIRS data is given in the appendix to this document by Nixon. It should be noted that the density (temperature) profile recovered from HASI data is sensitive towards the low end (300-150km) to some assumptions regarding the wind profile and the mass loss history due to ablation of the

heat shield that may not have been fully explored. Further, CIRS temperature retrieval and methane abundance profiles are typically coupled. Since the methane abundance in the stratosphere appears to be variable, it may be that CIRS data will not perfectly agree with the Huygens profile, although this remains an area for further study.

VIMS data relevant to the Huygens measurements pertain particularly to the haze optical properties and distribution. A recent Huygens-DISR / VIMS co-analysis is that by Griffith [15]. Note that early haze models to interpret DISR data alone (Tomasko et al., 2005; 2008) have been superseded by the more recent model [16]

VIMS data also yield information on methane abundance vs. altitude – the most comprehensive report to date is [17].

3. Upper Atmosphere Data

Before the Huygens parachute was deployed and descent began, the only data obtained was the Huygens Atmospheric Structure Instrument (HASI) entry deceleration profile, which can be inverted (with assumptions about the delivery state and wind profile) into a mass density profile and (assuming hydrostatic equilibrium) a temperature profile. These profiles may be compared with Cassini data, noting that the caveats above regarding latitude, season etc. apply more strongly in the more variable upper atmosphere. In particular, the growing Titan-Sun distance throughout the mission meant the atmosphere was cooling, and thus densities at high altitude progressively declined, such that the HASI profile has a higher density at a given altitude (e.g. 1200km) than almost all Cassini measurements.

A re-assessment summary of early upper atmospheric density measurements is provided in the table below. When the INMS recalibration (see below) is taken into account, there is relatively good agreement between different datasets (within the ~factor of 2 variation for an individual instrument between flybys)

Early Titan Upper Atmospheric Densities Compared (Ralph Lorenz 6/20/2018)										
Instrument	Flyby	Date	Latitude	Local Solar Time	Longitude	Density @1175km	Density @1025km	Density @950km	Source	
			deg	* hr:min	*	kg/m3	kg/m3	kg/m3		
INMS	TA	2004-300	38	16:45	-88	1.00E-10			Yelle/TAMWG *2.2 per Teolis	
AACS	TA	2004-300	38	16:45	-88	1.80E-10			Sarani 2007	
INMS	TB	2004-348	49	17:10	-81	7.50E-11			Yelle/TAMWG *2.2 per Teolis	
UVIS	TB	2004-348	-36	23:00	40	1.00E-10	1.00E-09	3.60E-09	Yelle/TAMWG *2.2 per Teolis	
HASI	TC	2005-014	-8.9	10:04	186	1.25E-10	7.43E-10	1.86E-09	HASI Level 4 Product on PDS	
INMS	T5	2005-106	74	23:09	88	4.30E-11	3.00E-10	1.10E-09	Yelle/TAMWG *2.2 per Teolis	
AACS	T5	2005-106	74	23:09	88	7.40E-11	6.00E-10	1.70E-09	Sarani 2007	
AACS	T7	2005-250	-67	4:50		7.00E-11			Sarani 2007	
UVIS	T10	2006-015	-60	20:04	5	6.83E-11			Derived** from Koskinen N2	
AACS	T16	2006-203	85	2:24			6.00E-10	2.30E-09	Sarani 2007	
UVIS	T21	2006-346				8.01E-11	6.36E-10	1.36E-09	Koskinen N2+CH4	
* published values differ - NB in-situ values may sweep over a large lat/long/local time range										
Similarly the area probed by an occultation will be different from that probed in-situ on the same flyby										
** N2@1198km *1.02 (alt 1198->1175) *1.05 (N2 -> N2+CH4)										

An important caveat also exists with respect to the Cassini Ion and Neutral Mass Spectrometer (INMS). The calibration of this instrument was not fully characterized until later in the mission, e.g. [18] and care should be taken that INMS data products (or results from publications prior to ~2015) referring to absolute number densities of neutrals (and thus, mass densities) should be scaled by a factor of 2.2 (+/-23%) [Relative results, such as mixing ratios were not affected]. Relevant INMS data were acquired on TA and TB, and on T5

UVIS provides information on the upper atmosphere via solar and stellar occultations, via the EUV and FUV. Spacecraft pointing errors can cause difficulty in retrievals, particularly in the FUV channel where there are significant pixel-to-pixel sensitivity variations and these are generally more difficult to deal with in stellar occultations.

Data were acquired on the TB stellar occultation, just a month before Huygens, from which a CH4 profile was obtained e.g. [19]. The pointing during this occultation had some inaccuracies which degraded the data somewhat; however, deriving a mass density profile assuming the N2/CH4 abundance ratio (varying with altitude) from INMS gives results in reasonable agreement with AACS and Huygens data, although it should be noted that this profile is at rather high latitude.

The T21 profile in [20] is a reasonable match to Huygens profile (not too long afterwards datewise, and at a relevant latitude (36 S), and at local solar time which isn't too far off).

T10 (Capablo et al 2015) is closer in date, but had some pointing complications and was at higher latitude and different solar time. Koskinen notes that while T10 had pointing issues, it turns out that their effect can be removed with relative ease and confidence from solar occultations in the EUV channel of the UVIS instrument.

T10 solar occultation N2 profile and a stellar occultation EUV channel retrieval for T21 (unpublished) by Koskinen are provided in attached files. Note that the results in [21] are all from the FUV channel that probes lower altitudes (but N2 is not derivable from this channel).

In addition to the science instruments on Cassini, upper atmospheric densities could be derived from the Attitude and Articulation Control System (AACS) on Cassini, which had to use thrusters to counteract the disturbance torque from the atmosphere. A useful summary is [22]– it may be noted that the density measured (down to 1173km) on the first flyby TA (October 2004, 3 months before Huygens) was the highest measured during the mission.

References

1. Kazeminejad, B., et al., Huygens' entry and descent through Titan's atmosphere---Methodology and results of the trajectory reconstruction. Planetary and Space Science, 2007. 55: p. 1845- 1876.

2. Stiles, B.W., et al., Determining Titan's Spin State from Cassini RADAR Images. The Astronomical Journal, 2008. 135: p. 1669-1680.

3. Kazeminejad, B., D.H. Atkinson, and J.-P. Lebreton, Titan's new pole: Implications for theHuygens entry and descent trajectory and landing coordinates. Advances in Space Research,2011. 47: p. 1622-1632.

4. Meriggiola, R., et al., The rotational dynamics of Titan from Cassini RADAR images. Icarus, 2016. 275: p. 183-192.

5. Lunine, J.I., et al., Titan's diverse landscapes as evidenced by Cassini RADAR's third and fourthlooks at Titan. Icarus, 2008. 195: p. 415-433.

6. Soderblom, L.A., et al., Correlations between Cassini VIMS spectra and RADAR SAR images:Implications for Titan's surface composition and the character of the Huygens Probe Landing Site. Planetary and Space Science, 2007. 55: p. 2025-2036.

7. Soderblom, L.A., et al., Topography and geomorphology of the Huygens landing site on Titan.Planetary and Space Science, 2007. 55: p. 2015-2024.

8. Rodriguez, S., et al., Cassini/VIMS hyperspectral observations of the HUYGENS landing site onTitan. Planetary and Space Science, 2006. 54: p. 1510-1523.

9. Porco, C.C., et al., Imaging of Titan from the Cassini spacecraft. Nature, 2005. 434: p. 159 168.

10. Wye, L.C., et al., Electrical properties of Titan's surface from Cassini RADAR scatterometer measurements. Icarus, 2007. 188: p. 367-385.

11. West, R.D., et al., Cassini RADAR sequence planning and instrument performance. IEEE Transactions on Geoscience and Remote Sensing, 2009. 47(6): p. 1777-1795.

12. Lorenz, R.D., et al., Observations of the surface of Titan by the Radar Altimeters on the Huygens Probe. Icarus, 2016. 270: p. 248-259.

13. Schinder, P.J., et al., The structure of Titan's atmosphere from Cassini radio occultations. Icarus, 2011. 215: p. 460-474.

14. Flasar, F.M., et al., Titan's Atmospheric Temperatures, Winds, and Composition. Science, 2005. 308: p. 975-978.

15. Griffith, C.A., et al., Radiative transfer analyses of Titan's tropical atmosphere. Icarus, 2012. 218: p. 975-988.

16. Doose, L.R., et al., Vertical structure and optical properties of Titan's aerosols from radiancemeasurements made inside and outside the atmosphere. Icarus, 2016. 270: p. 355-375.

17. Maltagliati, L., et al., Titan's atmosphere as observed by Cassini/VIMS solar occultations: CH4, CO and evidence for C2H6 absorption. Icarus, 2015. 248: p. 1-24.

18. Teolis, B.D., et al., A Revised Sensitivity Model for Cassini INMS: Results at Titan. Space Science Reviews, 2015. 190: p. 47-84.

19. Shemansky, D.E., et al., The Cassini UVIS Stellar Probe of the Titan Atmosphere. Science, 2005. 308: p. 978-982.

20. Kammer, J.A., et al., Composition of Titan's upper atmosphere from Cassini UVIS EUV stellar occultations. Planetary and Space Science, 2013. 88: p. 86-92.

21. Koskinen, T.T., et al., The mesosphere and lower thermosphere of Titan revealed by Cassini/UVIS stellar occultations. Icarus, 2011. 216: p. 507-534.

22. Sarani, S. A Novel Methodology for Reconstruction of Titan Atmospheric Density Using Cassini Guidance, Navigation, and Control Data. in AIAA Guidance, Navigation and Control Conference and Exhibit. 2007.

Appendix A. Observations related to the Huygens Landing site

1. Comparison of ISS and Radar images with Huygens DISR data

Figure 1 presents an albedo map of the Huygens landing site that was derived from Huygens/DISR images. Both ISS imaging data and Radar data are overlain by this map in Figures 2 and 3, allowing comparison of surface albedo and roughness characteristics of the surrounding data with the Huygens albedo map.

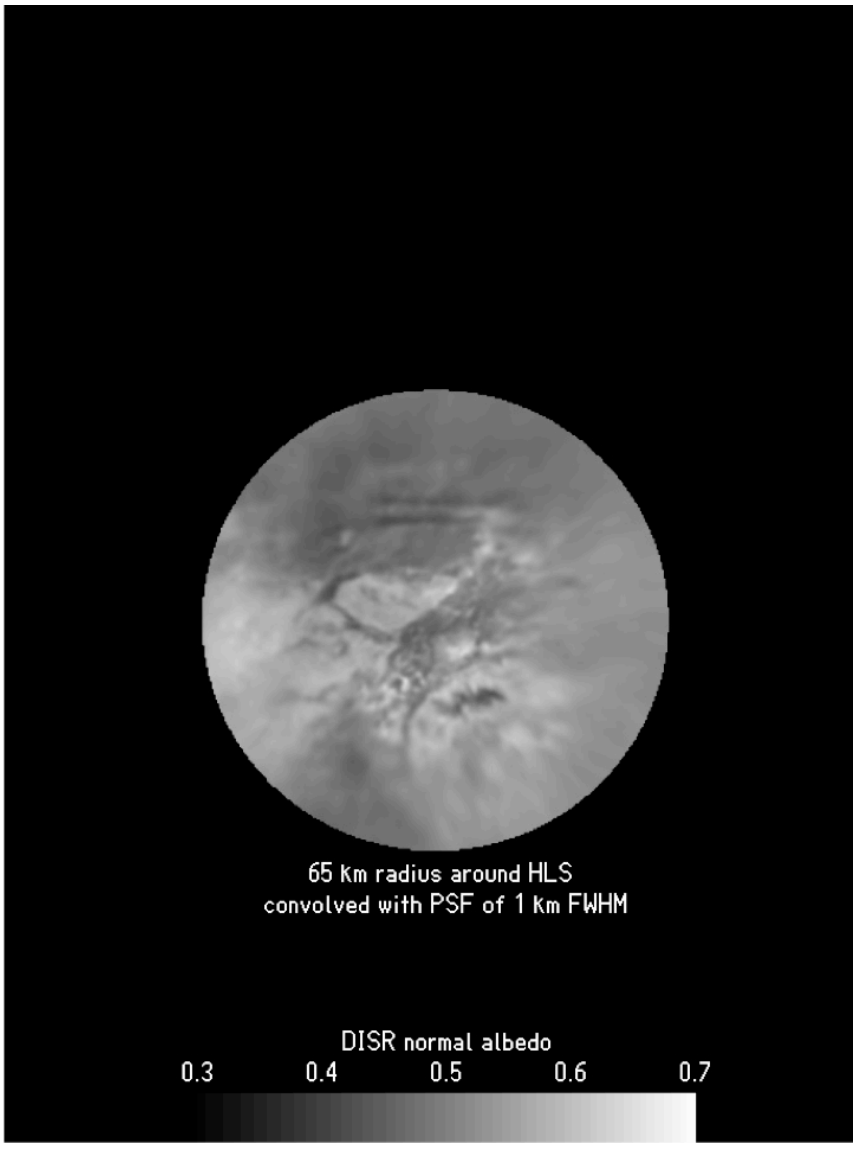

Figure 1. An albedo map if the area around the Huygens landing derived from DISR data.

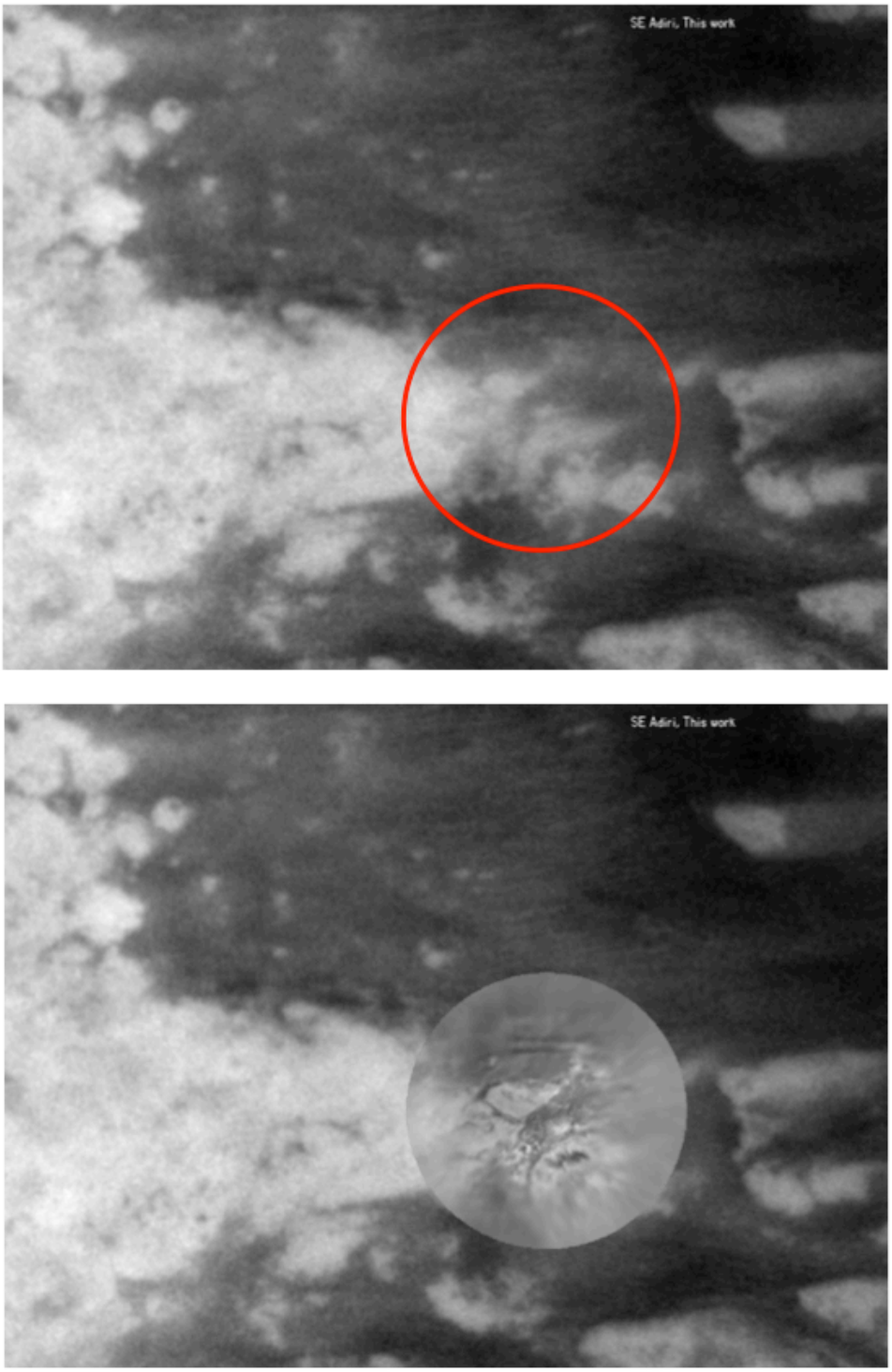

Figure 2. A comparison of CASSINI ISS (top) and Huygens DISR Data Bottom

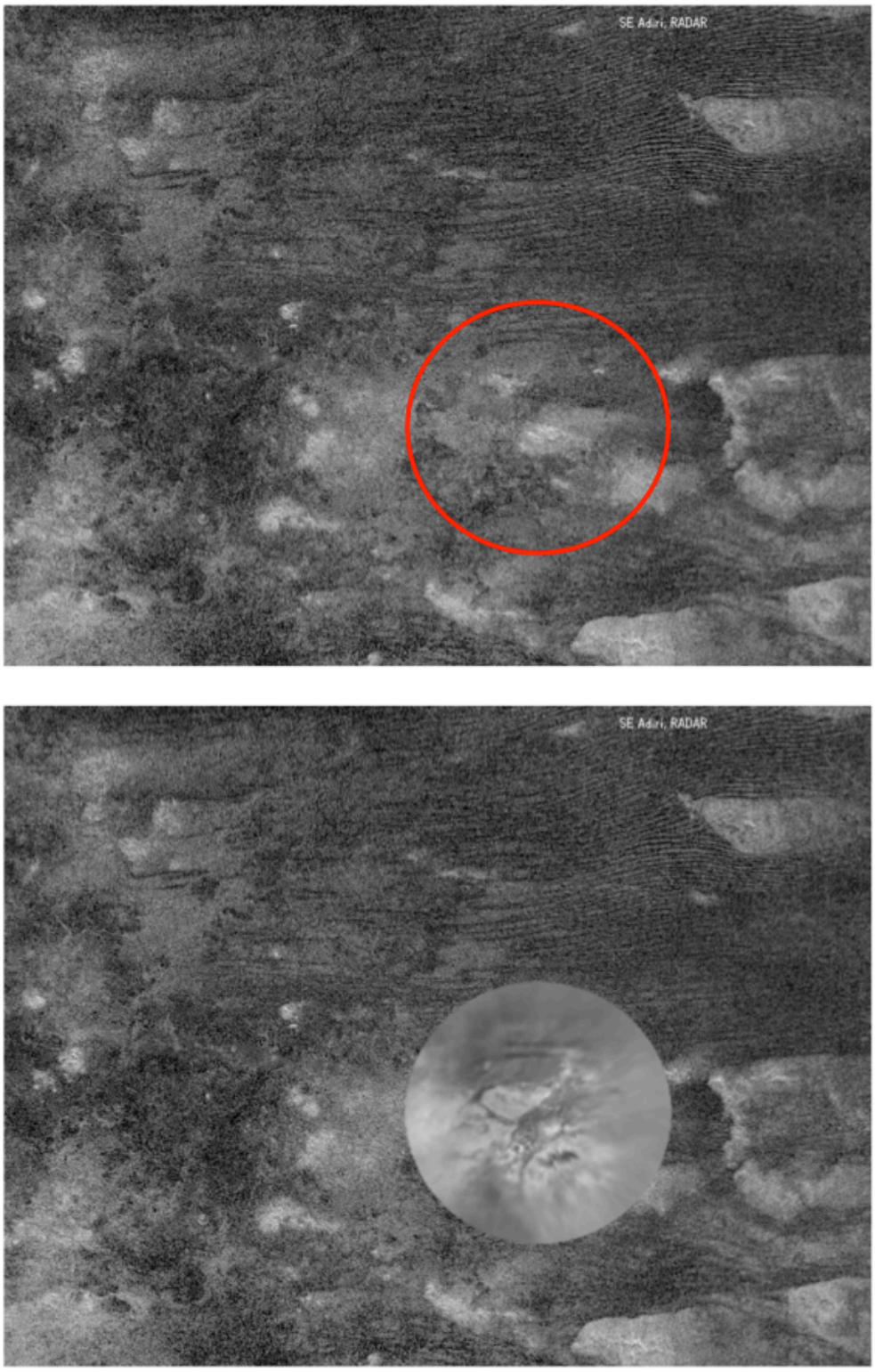

Figure 3. A comparison of Cassini RADAR (top) and Huygens DISR Data (Bottom)

2. Comparison of VIMS images with Huygens DISR data

flyby (T00A) before the probe landed on Titan. The observation was published in Rodriguez et al. (2006). Figure 4 below is extracted from that publication.

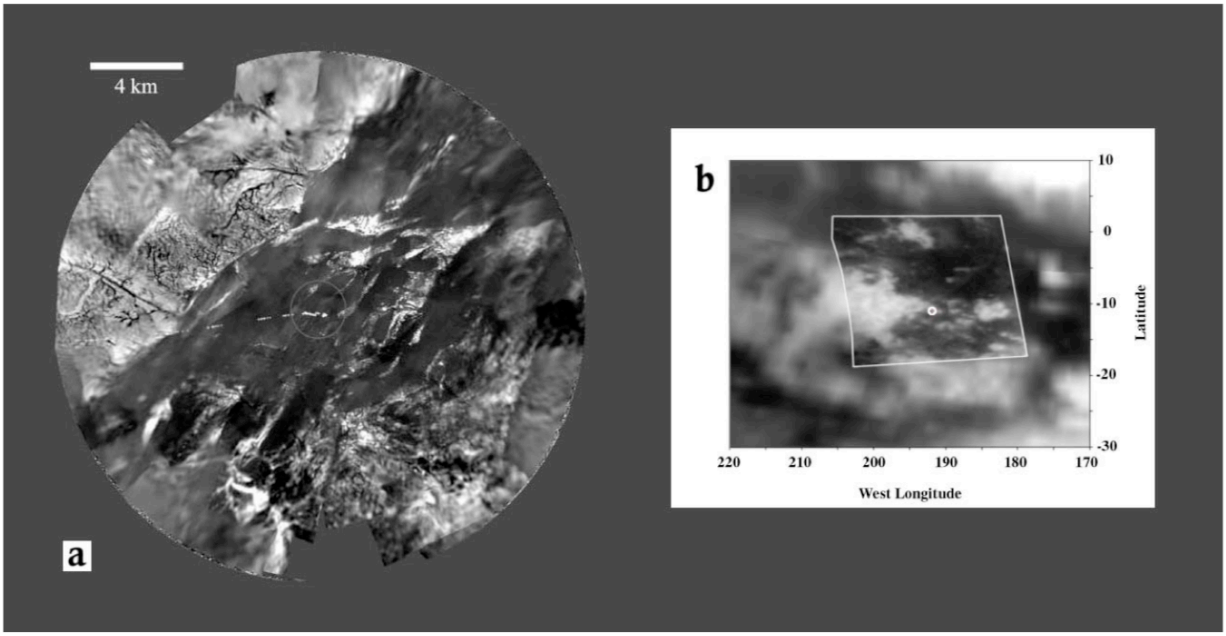

Figure 4. The comparison with the DISR mosaic acquired during the descent allowed us to determine precisely the location of the landing site.

Rodriguez, S., S. LeMouelic, C. Sotin, et al. (2006). Cassini VIMS Hyperspectral Observations of the Huygens Landing Site. Planetary and Space Science 54, 1510-1523.

A close observation of the Huygens Landing Site was acquired during flyby T047 (Figure 5). Comparison with the DISR mosaic acquired during the Huygens descent allowed a precise determination of the location of the landing site. During T47, a noodle mode was a also acquired as it was not possible to compensate for spacecraft motion at closest approach.

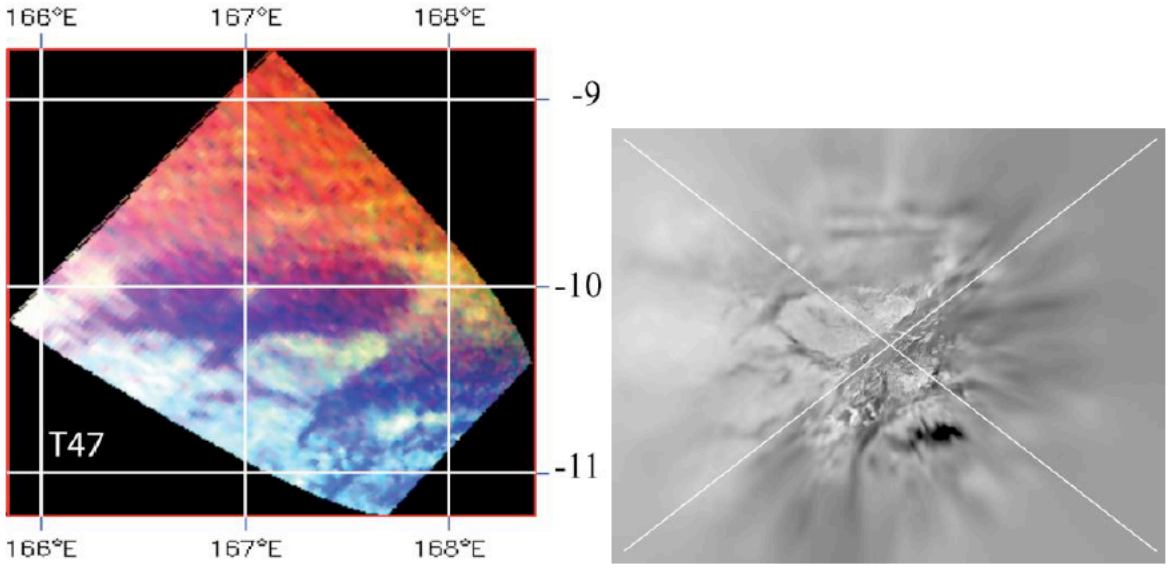

Figure 5. High resolution VIMS image of the Huygens Landing site (left) compared to the DISR image taken by the Huygens probe (right). The landing site is located at the intersection of the two white diagonals.

2. Radar Properties of the Huygens Landing Site

Ralph D Lorenz
Space Department, Johns Hopkins University Applied Physics Laboratory
And the CASSINI RADAR Team (Material from Cassini presentation, 2008)

Particular contributions from Mike Janssen, Bryan Stiles, Yanhua Anderson, Flora Paganelli, Richard West, Jonathan Lunine, Lauren Wye and Howard Zebker are noted. Huygens Probe Radar altimeter data were are available on the ESA PSA and the PDS Atmospheres node and are discussed in Lorenz R..D., Svedhem H., Trautner R., Kofman W., Herique A., Plettemeier D., Lebreton J.-P., Witasse O., Falkner P., Floury N., Ferri F., 2016. Observations of the Surface of Titan by the Radar Altimeters on the Huygens probe, Icarus, 270, 248-259

The following sequence of figures characterize the radar properties of the Huygens Landing site.

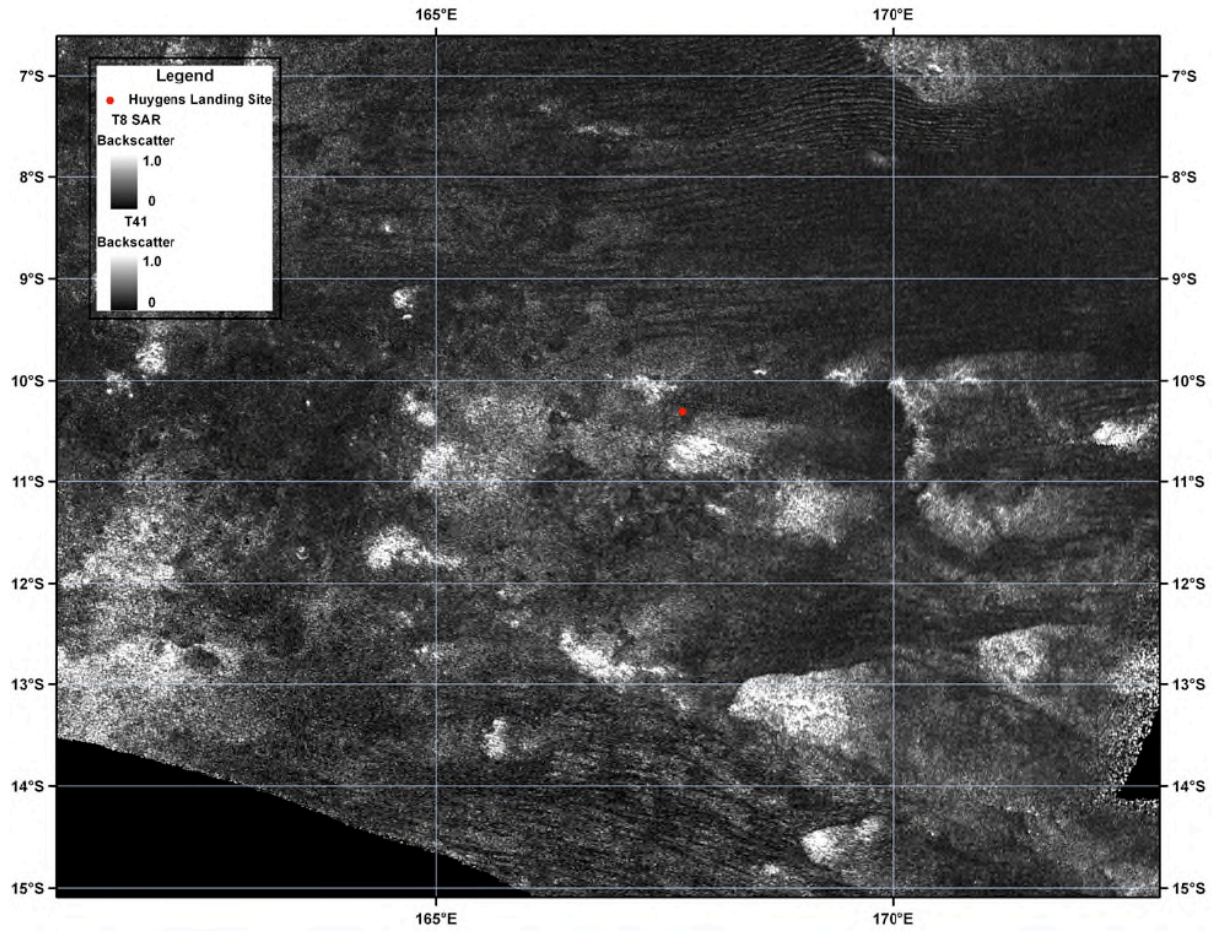

Figure 6. T8 SAR swath (due to M. Malaska) with lat-long grid (good to <0.3 deg)

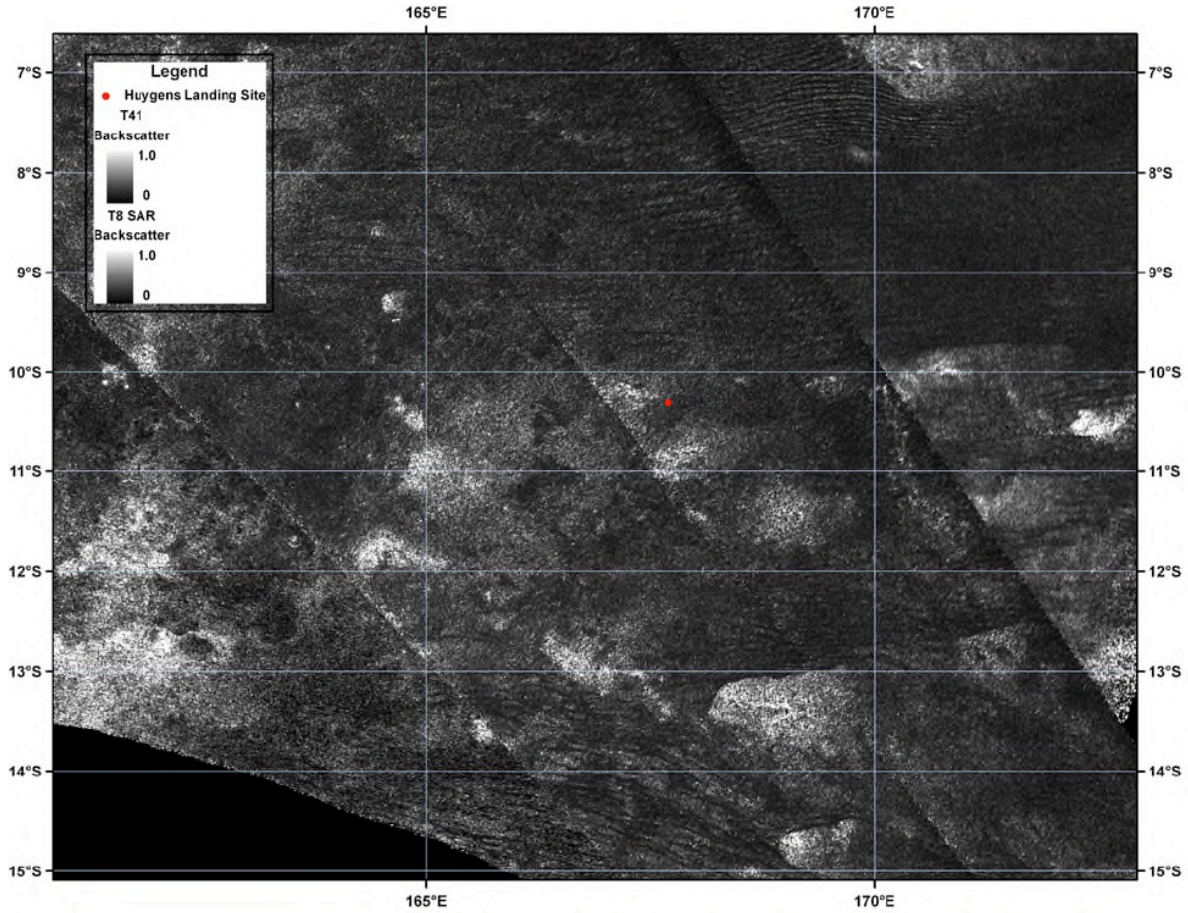

Figure 7. T8 SAR swath with T41 SAR superposed) - M. Malaska

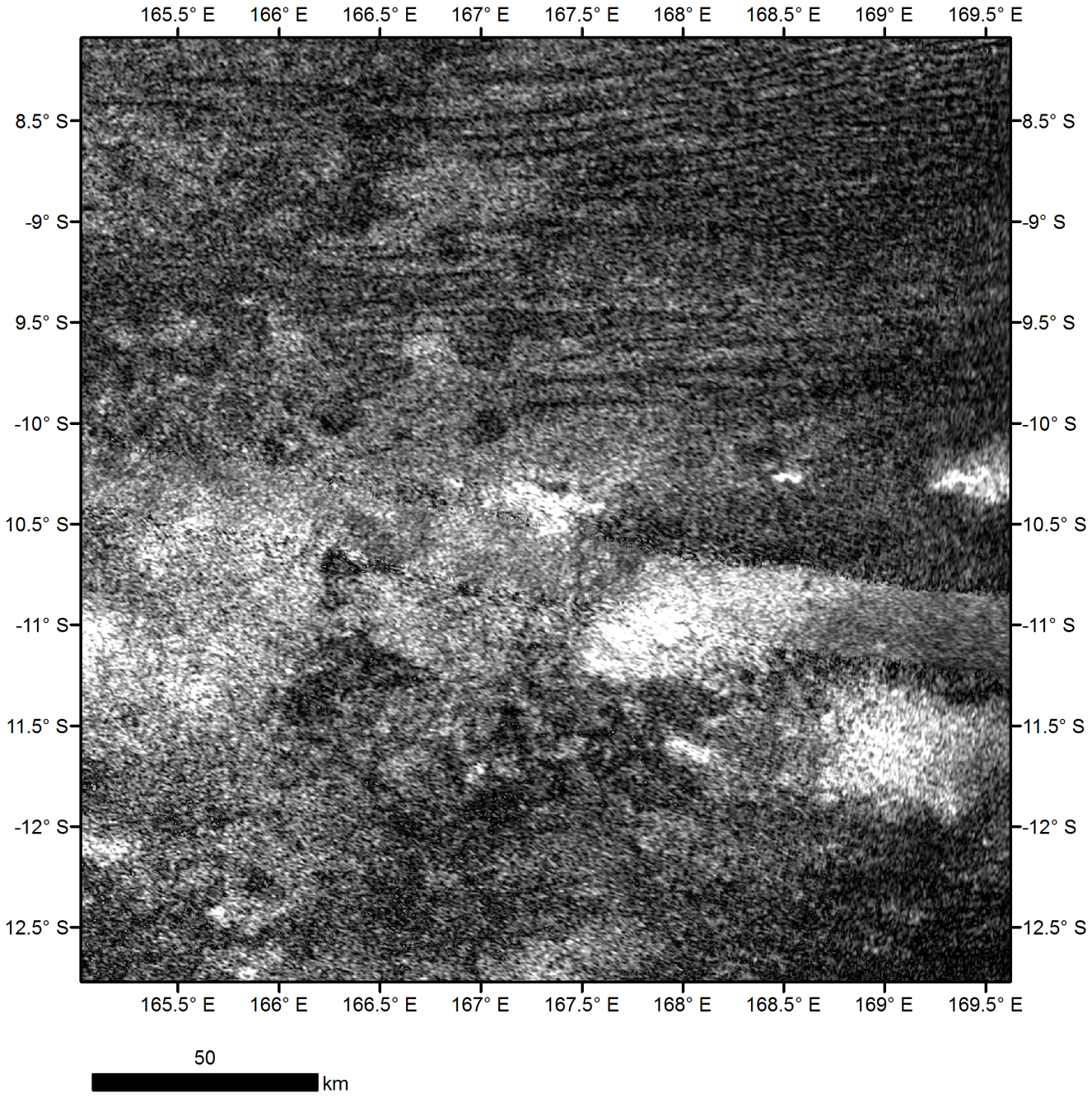

Figure 8. Huygens over T8 SAR

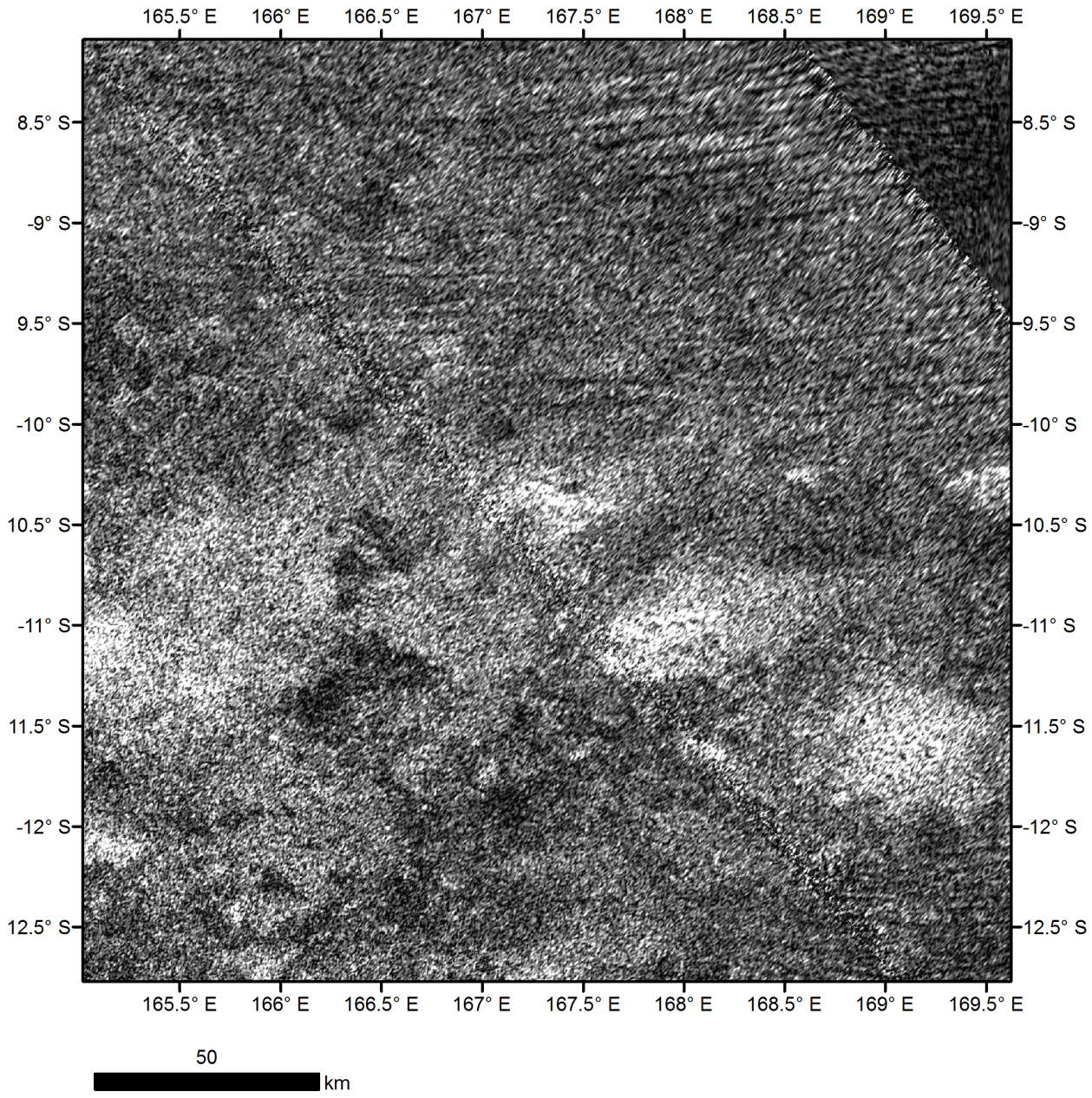

Figure 9. Huygens over T41 SAR

The Huygens landing site was the target of inbound scatterometry and radiometry observations on the first close flyby of Titan, TA (Oct 2004) (Figure 10). These data indicate landing site had backscatter between that of the dark plains and bright Xanadu. Radiometer data was similarly intermediate between cool Xanadu and warm Shangri-La . However, small-scale heterogeneity was evident so no firm expectations of liquid or not could be drawn for the probe.

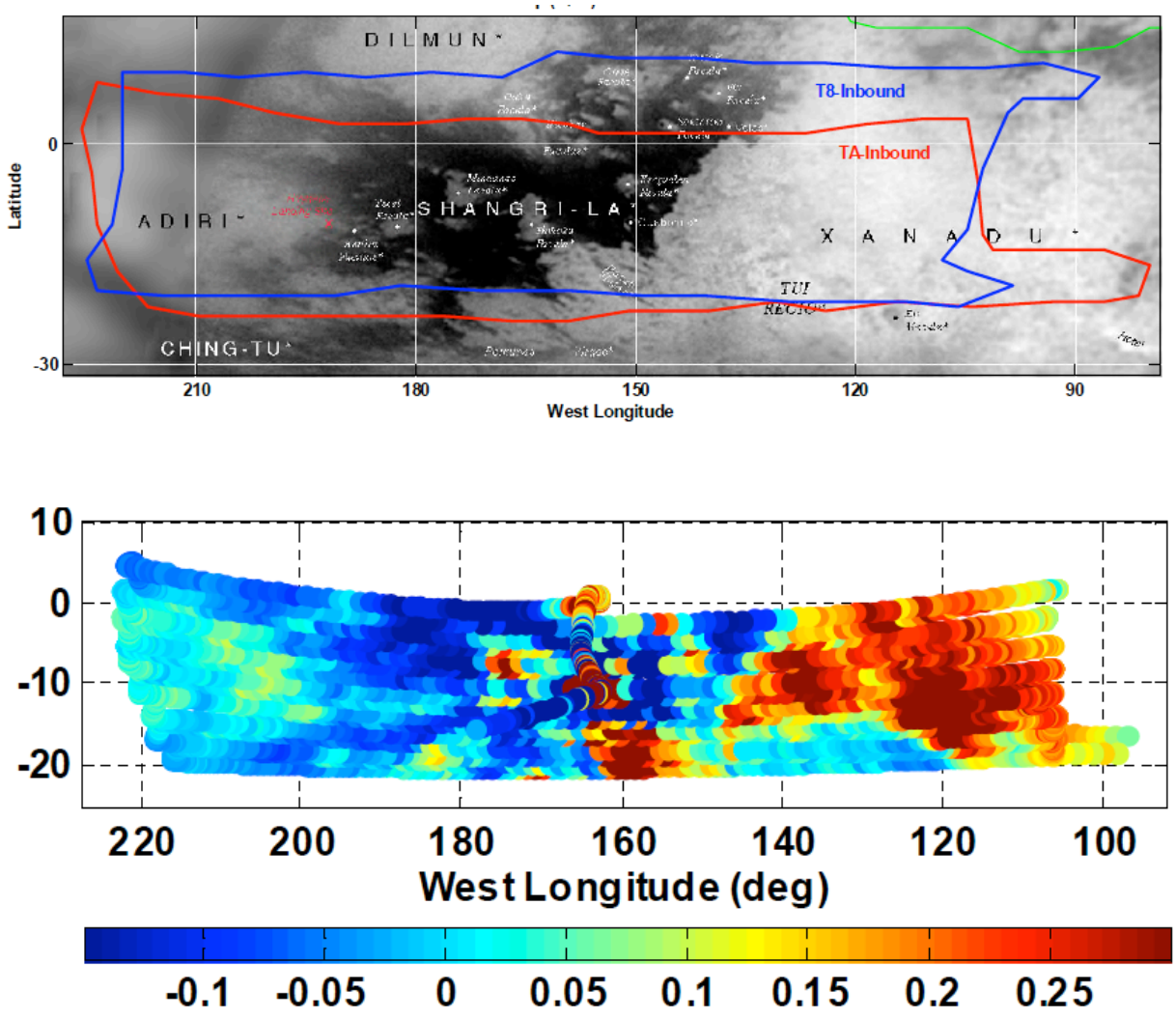

Figure 10. Scatterometry results over the Huygens langing site during TA (Oct. 2004)

Scatterometry data is discussed in Wye et al, Icarus, 2007

Scatterometer bursts were obtained over the Huygens landing site during the TA and T8 flycover. The T8 0bservation was closest to the site (see figure 11 - T8 (brown) This burst has a sigma0 value of 0.3547 at an incidence angle of 34.02 degrees. The footprint is about 98km in diameter (i.e. about 2 degrees across – the size of plot in Figure 11) and the polarization angle was 67 degrees.

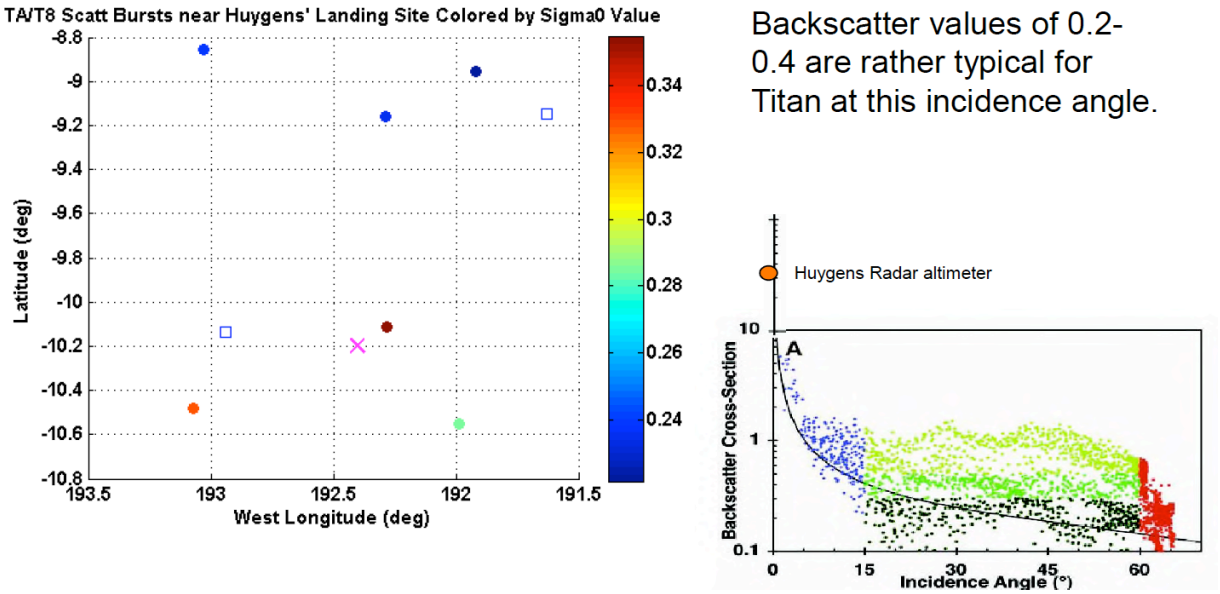

Figure 11. Ta and T8 Scat bursts near the Huygens Landing site

High resolution radiometry was obtained duringT8 and is shown in Figure 12, 13 and 14.

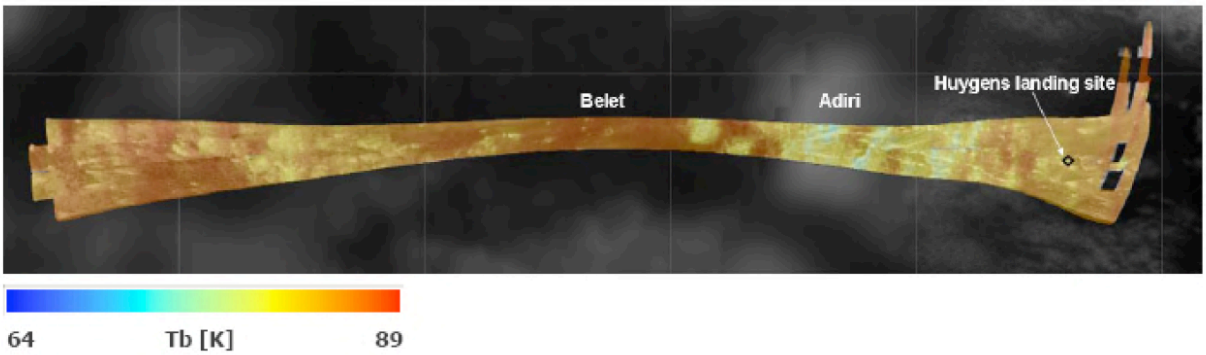

Figure 12. High-resolution' real-aperture radiometry obtained during T8 SAR swath shows landing site area to be rather 'cooler' than dune-covered areas like Belet, but warmer than Xanadu (*Paganelli et al. Icarus 2007*)

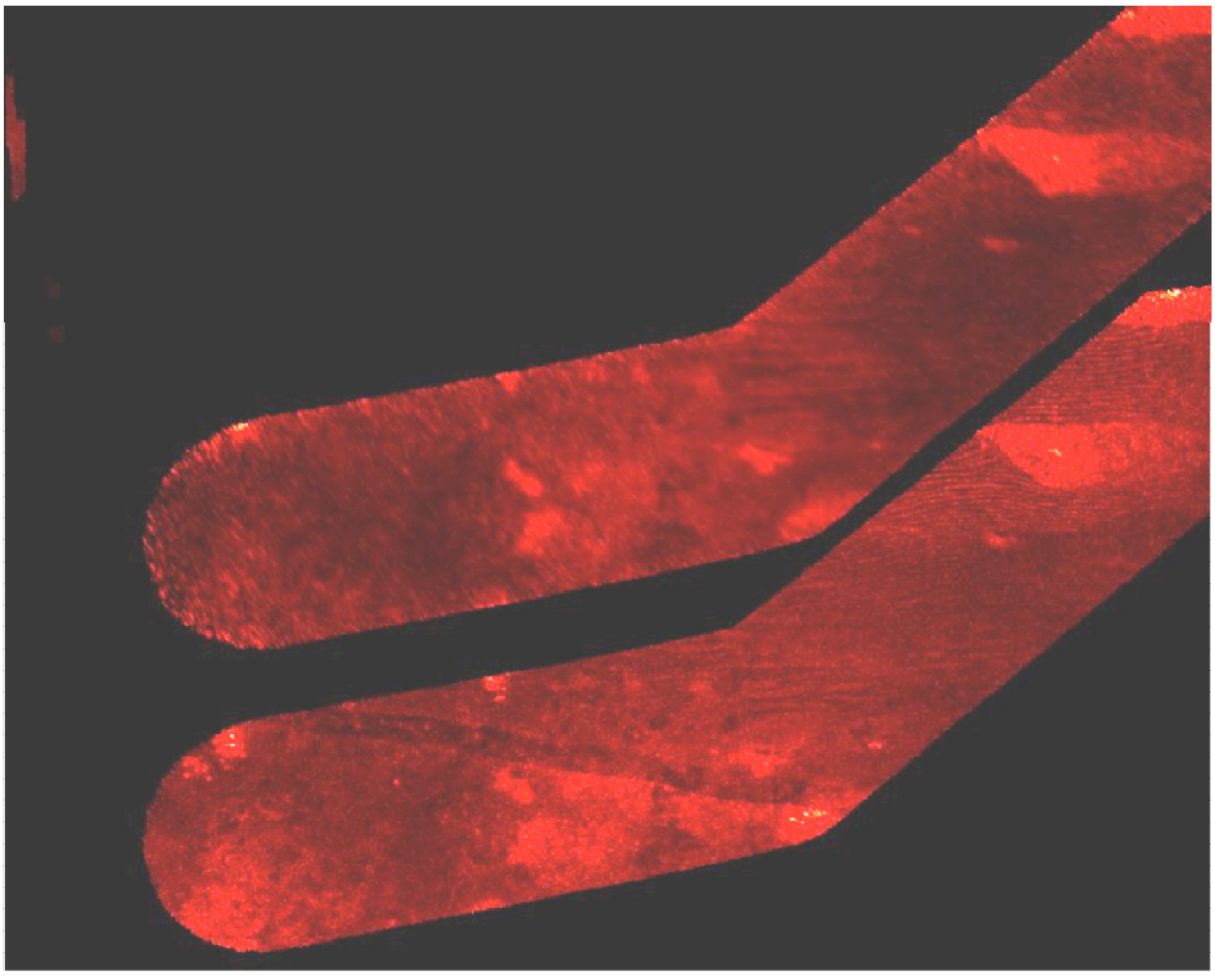

Figure 13. The T13 HiSAR swath (above) and the T8 swath (below, degraded in resolution to ~800m and masked to only show the area observed in T13). The correspondence of bright and dark features is very good. Some notable differences are the stripe across the center of T8 due to mismatch of the gains applied during processing and the fact that several linear features at upper left are clearly resolved in T8 but degrade into an overall dark region in T13.

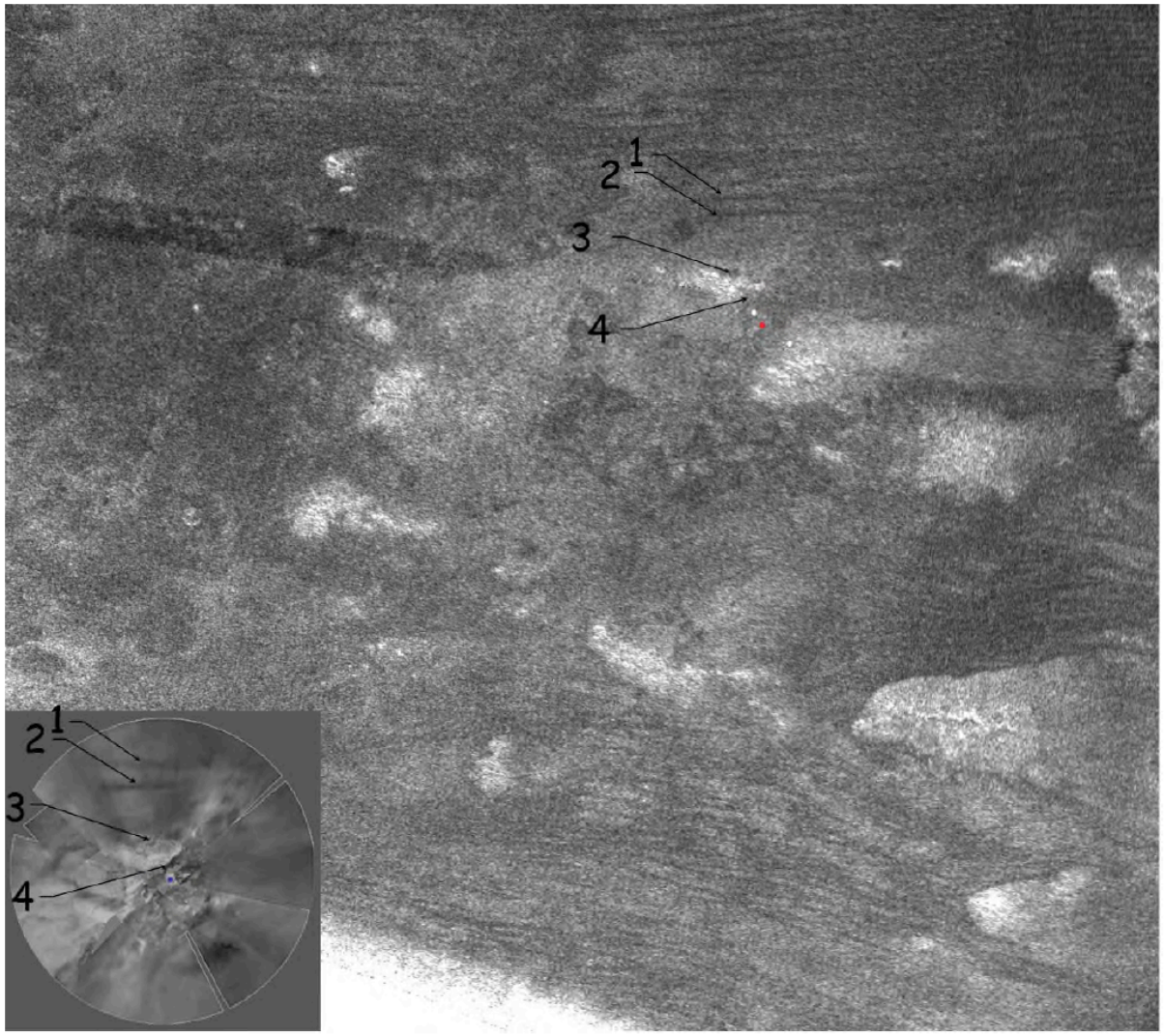

Figure 14. Numbered features were used to match T8 SAR observation to Huygens DISR mosaic (inset). The dunes 1&2 were instrumental, as there is not universal correlation of optical and radar brightness. (*Lunine et al., Icarus DISR mosaic courtesy of DISR team*)

3. RSS Observations related to the Huygens Site

An RSS Occultation was obtained in T12 on March 2006. Table 1 is from Schinder et al. Icarus 2011. Ingress occurred at 31.4^{o} S and egress at 52.8^{o} S.

Table 1.

		Ingress			Egress	
Altitude	Temp(k)	Pressure(mbar)	Refractivity	Temp(k)	Pressure(mbar)	Refractivity
300.0	185	0.09	0.004	185	0.09	0.004
290.0	185.6	0.11	0.005	185.18	0.11	0.005
280.0	184.24	0.13	0.006	185.02	0.13	0.006
270.0	183.65	0.16	0.007	181.62	0.16	0.007
260.0	182.69	0.2	0.009	179.89	0.19	0.009
250.0	181.04	0.25	0.011	178.7	0.24	0.011
240.0	179.36	0.3	0.014	178.52	0.3	0.013
230.0	178.42	0.38	0.017	178.54	0.37	0.016
220.0	176	0.47	0.021	176.82	0.45	0.021
210.0	174.03	0.58	0.027	174.06	0.57	0.026
200.0	172.3	0.73	0.034	172.86	0.71	0.033
195.0	171.25	0.82	0.038	171.63	0.79	0.037
190.0	170.48	0.92	0.043	169.94	0.89	0.042
185.0	169.53	1.03	0.049	168.41	1	0.048
180.0	168.79	1.16	0.055	166.67	1.12	0.054
175.0	167.63	1.3	0.062	166.76	1.27	0.061
170.0	166.03	1.47	0.071	165.73	1.43	0.069
165.0	164.81	1.66	0.081	164.24	1.61	0.079
160.0	163.75	1.87	0.092	163.03	1.82	0.09
155.0	162.1	2.12	1.005	162.81	2.06	1.002
150.0	160.77	2.4	1.02	160.31	2.34	1.017
145.0	158.99	2.72	1.037	158.97	2.65	1.034
140.0	156.64	3.1	1.059	156.97	3.02	1.054
135.0	155.97	3.53	1.082	155.15	3.44	1.078
130.0	153.88	4.03	2.01	153.7	3.93	2.005
125.0	152.16	4.61	2.043	151.56	4.49	2.038
120.0	150.64	5.29	2.081	149.05	5.16	2.077
115.0	148.07	6.07	3.029	146.07	5.93	3.026
110.0	145.74	7	3.085	143.04	6.85	3.084
105.0	143.84	8.08	4.051	141.07	7.94	4.051
100.0	140.77	9.36	5.034	138.2	9.23	5.036
95.0	137.7	10.89	6.035	136.08	10.76	6.034
90.0	133.99	12.73	7.062	132.2	12.59	7.064

85.0	130.19	14.94	9.021	128.78	14.81	9.023
80.0	124.54	17.65	11.037	123.74	17.51	11.035
75.0	117.28	21.07	14.041	117.86	20.94	14.026
70.0	109.24	25.45	18.068	112.57	25.16	17.093
65.0	87.87	31.64	28.092	94.65	31.03	26.032
60.0	75.41	41.44	44.016	77.11	40.07	41.076
55.0	71.85	55.82	62.051	71.17	53.95	60.098
50.0	70.57	75.95	86.07	69.79	73.66	85.003
48.0	70.39	85.91	98.038	69.52	83.44	96.076
46.0	70.26	97.46	111.089	69.54	94.94	110.013
44.0	70.2	110.63	127.023	69.49	107.72	125.015
42.0	70.27	125.33	144.011	69.53	122.07	141.086
40.0	70.36	142.22	163.046	69.49	138.58	161.028
38.0	70.58	161.55	185.03	69.76	157.57	182.088
36.0	70.78	183.04	209.06	70.14	179.01	206.087
34.0	71.09	207.65	237.004	70.54	203.39	233.097
32.0	71.61	235.11	266.077	71.1	231.12	264.014
30.0	72.18	265.37	299.011	71.71	261.98	297.025
28.0	72.89	301.92	337.05	72.5	296.26	332.097
26.0	73.77	341.91	378.02	73.38	333.48	370.08
24.0	74.64	385.97	422.062	74.51	378.56	415.012
22.0	75.74	435.47	470.063	75.53	428.36	464.011
20.0	76.86	488.71	521.025	76.49	481.4	515.091
19.0	77.56	519.52	549.049	77.17	513.06	545.049
18.0	78.43	559.84	586.01	77.78	544.09	574.039
17.0	78.85	580.59	604.091	78.47	574.97	602.012
16.0	79.48	617.85	639.028	79.31	609.23	631.054
15.0	80.21	660.01	677.031	80.06	648.52	666.06
14.0	80.79	692.66	706.025	80.56	684.04	699.04
13.0	81.53	737.01	745.041	81.13	720.48	732.009
12.0	82.08	778.35	782.064	81.83	767.61	774.017
11.0	82.76	824.27	822.082	82.58	813.34	813.047
10.0	83.36	864.69	857.077	83.32	857.82	851.018
9.5	84.15	919.23	904.001	83.76	884.91	873.073
9.0	84.2	922.76	906.092	84.05	902.63	888.041
8.5	84.33	930.58	913.035	84.53	934	914.058
8.0	84.93	966.87	942.078	84.81	954.17	931.059
7.5	85.48	998.64	968.011	85.45	996.9	966.067
7.0	85.98	1026.16	989.038	85.64	1009.6	976.092
6.5	86.5	1061.55	1017.082	86.02	1034.95	997.039
6.0	86.69	1076.97	1030.062	86.44	1063.61	1020.054
5.5	87.13	1113.35	1060.071	86.87	1093.77	1044.095
5.0	87.51	1142.91	1084.071	87.39	1131.28	1074.089

4.5	87.94	1170.96	1106.021	87.81	1160.1	1097.035
4.0	88.51	1205.48	1131.089	88.21	1186.26	1117.038
3.5	89.04	1237.81	1155.063	88.79	1223.21	1145.008
3.0	89.64	1274.22	1182.009	89.29	1254.6	1168.023
2.5	90.19	1305.96	1204.031	89.76	1284.05	1189.068
2.0	90.73	1335.3	1224.024	90.54	1328.64	1220.073
1.8	91.14	1357.03	1238.066	90.73	1339.5	1228.026
1.5	91.46	1373.5	1249.038	90.82	1344.83	1231.096
1.3	91.8	1390.88	1260.054	91.16	1365.18	1246.013
1.0	92.17	1409.95	1272.076	91.64	1396.97	1268.073
0.8	92.51	1427.57	1284.004	91.81	1409.42	1277.086
0.5	92.81	1443.93	1294.054	91.97	1422.2	1287.029
0.3	93.15	1466.08	1309.09	92.23	1442.94	1302.065
0.0	93.14	1467.93	1311.07	92.55	1468.49	1321.066
-0.3	.	.	.	92.64	1482.13	1332.939

4. UVIS Observations related to the Huygens Site

Number densities for N2 as a function of altitude is available for T10 (Table 2) and number densities of N_2 and CH_4 (Tables 3 and 4) are included for T21.

Table 2 Nitrogen Number Densities for T10

altitude(km)	nden(cm-3)	sigma_nden(cm-3)	alt resol(km)
1550.49	1.73677311E+007	6.69014608E+006	35.92
1538.86	1.80709289E+007	6.59735486E+006	37.38
1527.24	1.94021412E+007	6.60477401E+006	40.04
1515.64	2.36187584E+007	6.68420457E+006	38.01
1504.05	2.83595057E+007	6.77568113E+006	38.87
1492.49	3.03049106E+007	6.80861344E+006	38.80
1480.93	3.43574704E+007	6.93911988E+006	38.90
1469.40	3.76647065E+007	7.00098105E+006	37.27
1457.89	4.35395989E+007	7.12702250E+006	37.04
1446.39	5.04880945E+007	7.24803068E+006	39.14
1434.91	5.74339306E+007	7.37069554E+006	37.36
1423.44	6.46081033E+007	7.53600728E+006	37.86
1412.00	6.98864234E+007	7.67540211E+006	35.69
1400.57	7.55253431E+007	7.85812397E+006	39.43
1389.16	8.30504571E+007	8.04635514E+006	35.38
1377.77	9.58486594E+007	8.25055258E+006	37.11
1366.40	1.17588523E+008	8.58427315E+006	34.09
1355.05	1.41237092E+008	8.98555446E+006	38.98
1343.72	1.57619241E+008	9.30324038E+006	33.57
1332.40	1.73866533E+008	9.72488344E+006	37.24
1321.11	1.98017584E+008	1.02926066E+007	32.42

1309.83	2.31049271E+008	1.08830113E+007	38.06
1298.57	2.76429253E+008	1.18168101E+007	31.75
1287.34	3.23600337E+008	1.27854114E+007	36.23
1276.12	3.71763448E+008	1.40275406E+007	30.83
1264.93	4.21981205E+008	1.55445086E+007	37.24
1253.75	4.77443255E+008	1.75037880E+007	28.87
1242.60	5.42177918E+008	1.97948054E+007	34.59
1231.46	6.33529432E+008	2.42944043E+007	24.59
1220.35	7.37505176E+008	2.84998887E+007	34.07
1209.26	8.82119871E+008	4.09836019E+007	26.80
1198.19	1.04828959E+009	5.98822385E+007	201.50

Table 3 Nitrogen Number Densities for T21

Altitude(km)	Nden (m-3)	Error (m-3)
963.6345	2.9110e+16	1.9511e+16
985.4816	2.4067e+16	1.1542e+16
1007.3321	1.3315e+16	6.8591e+15
1029.1859	1.3620e+16	5.8017e+15
1051.0428	1.0659e+16	3.8656e+15
1072.9028	9.2675e+15	3.0032e+15
1094.7659	8.0963e+15	2.3646e+15
1116.6320	6.2679e+15	1.6663e+15
1138.5010	4.5366e+15	1.1486e+15
1160.3729	3.3177e+15	9.3447e+14
1182.2476	1.6995e+15	6.2972e+14
1204.1251	1.0038e+15	4.4880e+14
1226.0053	7.8031e+14	3.4733e+14
1247.8881	7.9251e+14	2.8639e+14
1269.7735	7.3311e+14	2.6902e+14
1291.6615	5.4963e+14	1.8975e+14
1313.5520	3.8747e+14	1.3001e+14
1335.4449	2.4840e+14	9.2003e+13
1357.3402	1.3750e+14	8.5845e+13
1379.2379	6.8196e+13	6.4494e+13
1401.1378	5.2810e+13	4.2750e+13
1423.0401	6.3982e+13	3.8340e+13
1444.9445	5.5652e+13	2.9606e+13
1466.8512	2.7841e+13	1.5245e+13
1488.7599	2.0865e+13	8.8707e+12

Table 4 Methane Number Densities for T21

Alt(km)	Nden (m-3)	Error (m-3)
963.6345	3.4950e+14	1.0976e+13
985.4816	2.6875e+14	7.6619e+12
1007.3321	2.0996e+14	6.6990e+12
1029.1859	1.6359e+14	6.0967e+12
1051.0428	1.3456e+14	5.6586e+12
1072.9028	1.1084e+14	5.3660e+12
1094.7659	8.7162e+13	4.9407e+12
1116.6320	7.0858e+13	4.7734e+12
1138.5010	5.9077e+13	4.4605e+12
1160.3729	4.5452e+13	4.2466e+12
1182.2476	4.0279e+13	4.0839e+12
1204.1251	3.3622e+13	3.8834e+12
1226.0053	2.6064e+13	3.7620e+12
1247.8881	2.4404e+13	3.6413e+12
1269.7735	1.9487e+13	3.4057e+12
1291.6615	1.0811e+13	3.0391e+12
1313.5520	1.0392e+13	2.8346e+12
1335.4449	9.2986e+12	2.7299e+12
1357.3402	1.0438e+13	2.7198e+12
1379.2379	6.0855e+12	2.6492e+12
1401.1378	6.0178e+12	2.5071e+12
1423.0401	5.0657e+12	1.6064e+12
1444.9445	5.2175e+12	5.8057e+11

5. CIRS Observations related to the Huygens Site

CIRS Data for Huygens Landing Site
Conor Nixon
May 2018

a. Surface Temperature

CIRS measures surface temperatures primarily through the FIRNADMAP (prime) and EUVFUV (UVIS rider) observations, which scan cross-disk at low spectral resolution. (15.5 cm^{-1}). Additionally, more limited surface temperature coverage comes from FIRNADCMP (0.5 cm^{-1}) observations (sit-and-stare).

Regular surface temperature coverage of the Huygens probe landing latitude was obtained in the months surrounding the landing. Table 5 shows the interpolated temperatures from surface measurements archived in the PDS volumes, e.g.: (http://atmos.nmsu.edu/pdsd/archive/data/co-s-cirs-234-tsdr-v32/cocirs_0401/EXTRAS/SURFTEMP/TITAN/).

Table 5.

Date	Observation Name	Interpolated Temperature at 10.573 S
13-DEC-2004	00BTI_FIRNADMAP001_UVIS	94.56 ± 0.38
16-APR-2005	006TI_FIRNADMAP003_UVIS	94.17 ± 0.38

These temperatures may not be representative of the probe longitude location, or time or day. For further details of the measurements and analysis see: [*Cottini et al.*, 2012]

b. Atmospheric Temperature Profile

The temperture profile at 15°S near the probe landing site derived from CIRS data was published in [*Flasar et al.*, 2005].

Further atmospheric temperatures at a variety of latitudes have been retrieved from the methane v_4 band at 7 μm by [*Richard K. Achterberg et al.*, 2008; *R. K. Achterberg et al.*, 2011; *TEANBY et al.*, 2009; *Teanby et al.*, 2017; *Teanby et al.*, 2008a; *Teanby et al.*, 2010; *Teanby et al.*, 2006; *Teanby et al.*, 2008b; *Teanby et al.*, 2013; *Teanby et al.*, 2007; *Vinatier et al.*, 2010; *Vinatier et al.*, 2007a; *Vinatier et al.*, 2015]

Table 6 contains a temperature profile for (11°S, 110°E, June 4, 2010) is given below, from Vinatier et al. (2015).

Table 6

Altitude(km)	P(mbar)	T(K)	T_min	T_max
527.03	9.96E-04	159.65	157.33	161.97
517.29	1.21E-03	160.23	157.96	162.49
507.57	1.46E-03	160.89	158.68	163.1
497.87	1.77E-03	161.64	159.48	163.79
488.17	2.14E-03	162.56	160.52	164.61
478.49	2.58E-03	163.55	161.56	165.54
468.8	3.13E-03	164.58	162.65	166.52
459.11	3.78E-03	165.58	163.7	167.46
449.42	4.58E-03	166.39	164.56	168.21
439.75	5.54E-03	167.03	165.26	168.79
430.09	6.70E-03	167.36	165.64	169.07
420.46	8.11E-03	167.26	165.6	168.92
410.89	9.81E-03	166.77	165.17	168.38
401.39	1.19E-02	166.03	164.43	167.63
391.96	1.44E-02	165.24	163.69	166.79
382.61	1.74E-02	164.68	163.18	166.17
373.32	2.10E-02	164.66	163.27	166.04
364.07	2.55E-02	165.5	164.23	166.77
354.83	3.08E-02	167.17	166.01	168.33
345.57	3.73E-02	169.41	168.41	170.4
336.28	4.51E-02	171.55	170.72	172.38
326.96	5.46E-02	173.95	173.29	174.61
317.61	6.60E-02	176.3	175.75	176.86
308.22	7.99E-02	178.32	177.88	178.76
298.82	9.67E-02	180.02	179.63	180.41
289.4	1.17E-01	181.09	180.76	181.42
280	1.42E-01	181.6	181.27	181.93

270.64	1.71E-01	181.84	181.56	182.11
261.32	2.07E-01	181.84	181.62	182.07
252.05	2.51E-01	181.66	181.44	181.88
242.86	3.04E-01	181.27	181.05	181.49
233.77	3.67E-01	180.3	180.08	180.52
224.8	4.44E-01	179.36	179.19	179.52
215.95	5.38E-01	178.42	178.26	178.59
207.24	6.51E-01	176.91	176.74	177.07
198.67	7.87E-01	175.17	175.01	175.34
190.26	9.53E-01	173.16	173	173.33
182	1.15E+00	170.81	170.64	170.97
173.9	1.40E+00	167.92	167.76	168.09
165.96	1.69E+00	165.77	165.61	165.94
158.17	2.04E+00	162.84	162.61	163.06
150.55	2.47E+00	160.38	160.16	160.61
143.08	2.99E+00	157.82	157.6	158.05
135.75	3.62E+00	156.56	156.33	156.78
128.54	4.38E+00	154.74	154.41	155.07
121.47	5.30E+00	152.81	152.42	153.19
114.56	6.41E+00	149.26	148.87	149.64
107.85	7.76E+00	145.31	144.87	145.75
101.33	9.38E+00	140.98	140.32	141.64
96.91	1.07E+01	137.82	136.93	138.7

b. Gas Abundance Profile

Methane: A co-analysis of the mid (7 μm) and far-infrared (>50 μm) methane lines to simultaneously retrieve temperature and methane VMR was conducted by [*Lellouch et al.*, 2014]. This work showed that previous inconsistency with the Huygens HASI experiment [*Fulchignoni et al.*, 2005] could be mitigated by revising the equatorial methane abundance downwards to 1.0% - however at the cost of disagreeing with Huygens GCMS [*Niemann et al.*, 2010]. A re-analysis of DISR data by Rey et al. (2018) has shown agreement with the lower value for methane from CIRS.

Hydrogen: the hydrogen abundance at low latitudes was determined by [*Courtin et al.*, 2012] to be $(9.6 \pm 2.4) \times 10^{-4}$, in good agreement with the Huygens GCMS [*Niemann et al.*, 2010]

Minor gases: VMR profiles of many trace gas species (C_2H_2, C_2H_4, C_2H_6, CH_3C_2H, C_3H_8, C_4H_2, C_6H_6, HC_3N, HCN, C_2N_2) have been published by the CIRS team [*TEANBY et al.*, 2009; *Teanby et al.*, 2017; *Teanby et al.*, 2008a; *Teanby et al.*, 2010; *Teanby et al.*, 2006; *Teanby et al.*, 2008b; *Teanby et al.*, 2013; *Teanby et al.*, 2007; *Vinatier et al.*, 2010; *Vinatier et al.*, 2007a; *Vinatier et*

al., 2015] A retrieved gas abundance profile for HCN, C_2H_2, C_2H_6 at (11°S, 110°E, June 4 2010) is given below in table 3, from [*Vinatier et al.*, 2015].

Table 7

P(mbar)	q_C2H2	q_C2H6	q_HCN
9.96E-04	2.48E-06	1.24E-05	4.93E-07
1.21E-03	2.34E-06	1.28E-05	5.13E-07
1.46E-03	2.18E-06	1.32E-05	5.28E-07
1.77E-03	2.03E-06	1.35E-05	5.40E-07
2.14E-03	1.90E-06	1.38E-05	5.46E-07
2.58E-03	1.78E-06	1.40E-05	5.50E-07
3.13E-03	1.69E-06	1.41E-05	5.51E-07
3.78E-03	1.62E-06	1.41E-05	5.54E-07
4.58E-03	1.58E-06	1.40E-05	5.58E-07
5.54E-03	1.56E-06	1.38E-05	5.67E-07
6.70E-03	1.55E-06	1.36E-05	5.81E-07
8.11E-03	1.56E-06	1.33E-05	5.99E-07
9.81E-03	1.56E-06	1.30E-05	6.20E-07
1.19E-02	1.55E-06	1.27E-05	6.40E-07
1.44E-02	1.53E-06	1.24E-05	6.55E-07
1.74E-02	1.49E-06	1.21E-05	6.61E-07
2.10E-02	1.43E-06	1.19E-05	6.55E-07
2.55E-02	1.36E-06	1.17E-05	6.34E-07
3.08E-02	1.30E-06	1.15E-05	6.01E-07
3.73E-02	1.24E-06	1.14E-05	5.59E-07
4.51E-02	1.21E-06	1.13E-05	5.14E-07
5.46E-02	1.21E-06	1.12E-05	4.71E-07
6.60E-02	1.24E-06	1.11E-05	4.33E-07
7.99E-02	1.31E-06	1.10E-05	4.04E-07
9.67E-02	1.41E-06	1.09E-05	3.84E-07
1.17E-01	1.55E-06	1.08E-05	3.73E-07
1.42E-01	1.70E-06	1.08E-05	3.71E-07
1.71E-01	1.87E-06	1.08E-05	3.76E-07
2.07E-01	2.02E-06	1.10E-05	3.86E-07
2.51E-01	2.15E-06	1.14E-05	3.97E-07
3.04E-01	2.24E-06	1.18E-05	4.06E-07
3.67E-01	2.30E-06	1.22E-05	4.08E-07
4.44E-01	2.32E-06	1.25E-05	4.00E-07
5.38E-01	2.34E-06	1.26E-05	3.82E-07
6.51E-01	2.34E-06	1.24E-05	3.54E-07

7.87E-01	2.35E-06	1.20E-05	3.21E-07
9.53E-01	2.35E-06	1.14E-05	2.86E-07
1.15E+00	2.33E-06	1.07E-05	2.53E-07
1.40E+00	2.25E-06	1.00E-05	2.25E-07
1.69E+00	2.10E-06	9.35E-06	2.03E-07
2.04E+00	1.86E-06	8.68E-06	1.88E-07
2.47E+00	1.57E-06	8.00E-06	1.79E-07
2.99E+00	1.27E-06	7.34E-06	1.78E-07
3.62E+00	9.81E-07	6.72E-06	1.83E-07
4.38E+00	7.47E-07	6.22E-06	1.95E-07
5.30E+00	5.75E-07	5.88E-06	2.15E-07

c. Haze Profile

Low-latitude profiles of haze and condensates have been published by [*Anderson and Samuelson*, 2011; *Vinatier et al.*, 2010; *Vinatier et al.*, 2015; *Vinatier et al.*, 2012]

d. Isotopic Ratios

CIRS has measured many isotopic ratios including D/H (in CH_4, C_2H_2), $^{12}C/^{13}C$ (in CH_4, C_2H_2, C_2H_6, HCN, C_4H_2, HC_3N, CO_2), $^{14}N/^{15}N$ (in HCN), $^{16}O/^{18}O$ (in CO_2). For comparison to the Huygens isotopic ratios, the most important measured ratios by CIRS are:

Table 8

Ratio	Cassini CIRS	Reference	Huygens GCMS	Reference
D/H	CH4: $1.32\ (+0.15)\ (-0.11)\ \text{x}10^{-4}$	[*Bezard et al.*, 2007]	H2: (1.35 ± 0.30) 10E−4	[*Niemann et al.*, 2010]
$^{12}C/^{13}C$	CH4: 82 (+27/−18)	[*Bezard et al.*, 2007]	91.1 ± 1.4	[*Niemann et al.*, 2010]
$^{14}N/^{15}N$	HCN: 56 ± 8	[*Vinatier et al.*, 2007b]	167.7 ± 0.6	[*Niemann et al.*, 2010]

Note that the molecules that the ratios are measured in are often different. For a discussion, see review by Bezard et al. 2014.

References

Achterberg, R. K., B. J. Conrath, P. J. Gierasch, E. M. Flasar, and C. A. Nixon (2008), Titan's middle-atmospheric temperatures and dynamics observed by the Cassini Composite Infrared Spectrometer, *Icarus*, *194*(1), 263-277, doi:10.1016/j.icarus.2007.09.029.

Achterberg, R. K., P. J. Gierasch, B. J. Conrath, F. M. Flasar, and C. A. Nixon (2011), Temporal variations of Titan's middle-atmospheric temperatures from 2004 to 2009 observed by Cassini/CIRS, *Icarus*, *211*(1), 686-698, doi:10.1016/j.icarus.2010.08.009.

Anderson, C. M., and R. E. Samuelson (2011), Titan's aerosol and stratospheric ice opacities between 18 and 500 mu m: Vertical and spectral characteristics from Cassini CIRS, *Icarus*, *212*(2), 762-778, doi:10.1016/j.icarus.2011.01.024.

Bezard, B., C. A. Nixon, I. Kleiner, and D. E. Jennings (2007), Detection of (CH3D)-C-13 on Titan, *Icarus*, *191*(1), 397-400, doi:10.1016/j.icarus.2007.06.004.

Cottini, V., C. A. Nixon, D. E. Jennings, R. de Kok, N. A. Teanby, P. G. J. Irwin, and F. M. Flasar (2012), Spatial and temporal variations in Titan's surface temperatures from Cassini CIRS observations, *Planetary and Space Science*, *60*(1), 62-71, doi:10.1016/j.pss.2011.03.015.

Courtin, R., C. K. Sim, S. J. Kim, and D. Gautier (2012), The abundance of H-2 in Titan's troposphere from the Cassini CIRS investigation, *Planetary and Space Science*, *69*(1), 89-99, doi:10.1016/j.pss.2012.03.012.

Flasar, F. M., et al. (2005), Titan's atmospheric temperatures, winds, and composition, *Science*, *308*(5724), 975-978, doi:10.1126/science.1111150.

Fulchignoni, M., et al. (2005), In situ measurements of the physical characteristics of Titan's environment, *Nature*, *438*(7069), 785-791, doi:10.1038/nature04314.

Lellouch, E., B. Bezard, F. M. Flasar, S. Vinatier, R. Achterberg, C. A. Nixon, G. L. Bjoraker, and N. Gorius (2014), The distribution of methane in Titan's stratosphere from Cassini/CIRS observations, *Icarus*, *231*, 323-337, doi:10.1016/j.icarus.2013.12.016.

Niemann, H. B., S. K. Atreya, J. E. Demick, D. Gautier, J. A. Haberman, D. N. Harpold, W. T. Kasprzak, J. I. Lunine, T. C. Owen, and F. Raulin (2010), Composition of Titan's lower atmosphere and simple surface volatiles as measured by the Cassini-Huygens probe gas chromatograph mass spectrometer experiment, *Journal of Geophysical Research-Planets*, *115*, doi:10.1029/2010je003659.

TEANBY, N., P. IRWIN, R. DE KOK, and e. al. (2009), Dynamical implications of seasonal and spatial variations in Titan's stratospheric composition, *PHILOSOPHICAL TRANSACTIONS OF THE ROYAL SOCIETY A-MATHEMATICAL PHYSICAL AND ENGINEERING SCIENCES*, *367*(1889), 697-711, doi:10.1098/rsta.2008.0164.

Teanby, N. A., B. Bezard, S. Vinatier, M. Sylvestre, C. A. Nixon, P. G. J. Irwin, R. J. de Kok, S. B. Calcutt, and F. M. Flasar (2017), The formation and evolution of Titan's winter polar vortex, *Nature Communications*, *8*, doi:10.1038/s41467-017-01839-z.

Teanby, N. A., et al. (2008a), Titan's winter polar vortex structure revealed by chemical tracers, *Journal of Geophysical Research-Planets*, *113*(E12), doi:10.1029/2008je003218.

Teanby, N. A., P. G. J. Irwin, R. de Kok, and C. A. Nixon (2010), SEASONAL CHANGES IN TITAN'S POLAR TRACE GAS ABUNDANCE OBSERVED BY CASSINI, *Astrophysical Journal Letters*, *724*(1), L84-L89, doi:10.1088/2041-8205/724/1/l84.

Teanby, N. A., et al. (2006), Latitudinal variations of HCN, HC3N, and C2N2 in Titan's stratosphere derived from cassini CIRS data, *Icarus*, *181*(1), 243-255, doi:10.1016/j.icarus.2005.11.008.

Teanby, N. A., et al. (2008b), Global and temporal variations in hydrocarbons and nitriles in Titan's stratosphere for northern winter observed by Cassini/CIRS, *Icarus*, *193*(2), 595-611, doi:10.1016/j.icarus.2007.08.017.

Teanby, N. A., P. G. J. Irwin, C. A. Nixon, R. Courtin, B. M. Swinyard, R. Moreno, E. Lellouch, M. Rengel, and P. Hartogh (2013), Constraints on Titan's middle atmosphere ammonia abundance from Herschel/SPIRE sub-millimetre spectra, *Planetary and Space Science*, *75*, 136-147, doi:10.1016/j.pss.2012.11.008.

Teanby, N. A., et al. (2007), Vertical profiles of HCN, HC3N, and C2H2 in Titan's atmosphere derived from Cassini/CIRS data, *Icarus*, *186*(2), 364-384, doi:10.1016/j.icarus.2006.09.024.

Vinatier, S., et al. (2010), Analysis of Cassini/CIRS limb spectra of Titan acquired during the nominal mission II: Aerosol extinction profiles in the 600-1420 cm(-1) spectral range, *Icarus*, *210*(2), 852-866, doi:10.1016/j.icarus.2010.06.024.

Vinatier, S., et al. (2007a), Vertical abundance profiles of hydrocarbons in Titan's atmosphere at 15 degrees S and 80 degrees N retrieved from Cassini/CIRS spectra, *Icarus*, *188*(1), 120-138, doi:10.1016/j.icarus.2006.10.031.

Vinatier, S., et al. (2015), Seasonal variations in Titan's middle atmosphere during the northern spring derived from Cassini/CIRS observations, *Icarus*, *250*, 95-115, doi:10.1016/j.icarus.2014.11.019.

Vinatier, S., B. Bezard, and C. A. Nixon (2007b), The Titan N-14/N-15 and C-12/C-13 isotopic ratios in HCN from Cassini/CIRS, *Icarus*, *191*(2), 712-721, doi:10.1016/j.icarus.2007.06.001.

Vinatier, S., P. Rannou, C. M. Anderson, B. Bezard, R. de Kok, and R. E. Samuelson (2012), Optical constants of Titan's stratospheric aerosols in the 70-1500 cm(-1) spectral range constrained by Cassini/CIRS observations, *Icarus*, *219*(1), 5-12, doi:10.1016/j.icarus.2012.02.009.